PHILOSOPHICAL TRANSACTIONS OF THE ROYAL SOCIETY A

rsta.royalsocietypublishing.org

Research

Cite this article: Elishakoff I, Challamel N, Soret C, Bekel Y, Gomez T. 2013 Virus sensor based on single-walled carbon nanotube: improved theory incorporating surface effects. Phil Trans R Soc A 371: 20120424. http://dx.doi.org/10.1098/rsta.2012.0424

One contribution of 17 to a Theme Issue 'A celebration of mechanics: from nano to macro'.

Subject Areas:
nanotechnology

Keywords:
carbon nanotubes, nanosensors, Bresse–Timoshenko beams, non-local effects, surface effects

Author for correspondence:
Isaac Elishakoff
e-mail: elishako@fau.edu

Electronic supplementary material is available at http://dx.doi.org/10.1098/rsta.2012.0424 or via http://rsta.royalsocietypublishing.org.

Royal Society Publishing
Informing the science of the future

Virus sensor based on single-walled carbon nanotube: improved theory incorporating surface effects

Isaac Elishakoff[1], Noël Challamel[2], Clément Soret[3], Yannis Bekel[4] and Thomas Gomez[5]

[1]Department of Ocean and Mechanical Engineering, Florida Atlantic University, Boca Raton, FL 33431-0991, USA
[2]Laboratoire d'Ingénierie des MATériaux de Bretagne, Université de Bretagne Sud, Lorient Centre de, Recherche, Rue de Saint Maudé, BP 92116, 56321 Lorient, France
[3]Institut Français de Mécanique Avancée, 63170 Aubière, France
[4]Ecole Centrale Paris, 92290 Châtenay-Malabry, France
[5]Département Génie Civil, Ecole Polytech Clermont-Ferrand, Université Blaise Pascal, 63170 Aubière, France

In this paper, we deal with the theoretical framework for a single-walled carbon nanotube serving as a virus or bacterium sensor, with the complicating influences of non-locality and surface effects taken into account. It is demonstrated that these effects are not negligible as is often assumed in the literature; they may greatly influence both the vibration behaviour as well as the identification process of the virus or bacterium.

1. Analysis

As Tibbals [1] writes: 'nanomedicine and medical nanotechnology are taking an interesting and promising direction. The terms "nanomedicine" and "medical nanotechnology" have been formally established since their adoption into major programme initiatives by the National Institutes of Health and other leading medical bodies worldwide' (see also Koprowski [2]). In this respect, the contribution of nanotechnology to the mitigation of serious virus outbreaks that may develop into pandemics lies, in part, in the development of nanosensors that may detect the presence of a virus.

The interested reader may consult the books by Jha [3], Khanna [4] and Lim [5], for example. Current nanotechnology offers several new possibilities for the development of sensing possibilities with a view to detecting a virus or bacterium. Several authors used refined theory to describe vibrations of short carbon nanotubes, including the effects of shear deformation and rotary inertia, leading to application of the refined Bresse–Timoshenko theory rather than the classical Bernoulli–Euler theory. However, at the small scale, there are additional effects that ought to be taken into account. In this respect, one has to mention the non-local continuum mechanics that allows one to account for the small-length-scale effects that become quite important when dealing with nanostructures. Considerable interest has been demonstrated recently in the application of non-local continuum mechanics for proper modelling of microbeams and nanobeams. Lu *et al.* [6,7] proposed a generalization of the Bresse–Timoshenko equations for flexural beams to be analysed by the non-local theory. However, they did not include surface effects. Lee & Chang [8] (see also [9,10]) proposed a generalization of the Bresse–Timoshenko equations for flexural beams analysed by the non-local theory with surface effects:

$$(EI)^* \frac{\partial^2 \phi}{\partial x^2} + \kappa GA\left(\frac{\partial v}{\partial x} - \phi\right) - \left[1 - (e_0 a)^2 \frac{\partial^2}{\partial x^2}\right] \rho I \frac{\partial^2 \phi}{\partial t^2} = 0 \tag{1.1}$$

and

$$\kappa GA\left(\frac{\partial^2 v}{\partial x^2} - \frac{\partial \phi}{\partial x}\right) - \left[1 - (e_0 a)^2 \frac{\partial^2}{\partial x^2}\right]\left[\rho A \frac{\partial^2 v}{\partial t^2} - \frac{\partial}{\partial x}\left(H \frac{\partial v}{\partial x}\right)\right] = -\left[p - (e_0 a^2) \frac{\partial^2 p}{\partial x^2}\right]. \tag{1.2}$$

Here κ is the shear coefficient that depends on the shape of the cross section, A is the area of the cross section, G is the modulus of elasticity in shear, ϕ is the slope of the deflection curve when the shear force is neglected, v is the total deflection, x is the axial displacement, ρ is the mass density per unit volume, t is the time, E is the Young's modulus of elasticity, I is the area moment of inertia, $(EI)^*$ is the effective flexural rigidity that includes the surface bending elasticity on the nanotube and its flexural rigidity and is defined as $(EI)^* = \pi E^S (R_i^3 + R_o^3) + EI$, with E^S being the surface elasticity modulus, H is a constant parameter that is determined by the residual surface tension and the shape of the cross section and is defined as $H = 4\tau(R_i + R_o)$ with τ the residual surface tension per unit length on the nanotube, $e_0 a$ is the scale coefficient that incorporates the non-locality effect, a is an internal characteristic length, e_0 is a constant for adjusting the model in matching some reliable results by experiments or other models, and $p(x)$ is the distributed load that may set on the beam (in free vibration, we set $p(x) = 0$). When $e_0 a = 0$, and in the absence of surface elasticity effects, equations (1.1) and (1.2) are reduced to the equations of the classical Bresse–Timoshenko beam.

A more refined model has been given recently by Ansari & Sahmani [11] for different local beam theories, including the Bresse–Timoshenko beam theory. Hereinafter, we extend the earlier-mentioned theory for the non-local beam.

Note that the model of Lu *et al.* [6] or Lu *et al.* [7] is valid for a surface elasticity loading modelled as a conservative loading. The reader is referred also to the recent study of Challamel & Elishakoff [12] for a discussion on conservative versus non-conservative modelling of surface elasticity effects.

It was shown by Elishakoff [13] that a simpler and more consistent set of equations is derivable by retaining equation (1.2), whereas equation (1.1) should be replaced by

$$(EI)^* \frac{\partial^2 \phi}{\partial x^2} + \kappa GA\left(\frac{\partial v}{\partial x} - \phi\right) - \left[1 - (e_0 a)^2 \frac{\partial^2}{\partial x^2}\right] \rho I \frac{\partial^3 v}{\partial x \partial t^2} = 0. \tag{1.3}$$

We put equations (1.2) and (1.3) in the form

$$M_{11} v(x,t) + M_{12} \phi(x,t) = 0 \tag{1.4}$$

and

$$M_{21} v(x,t) + M_{22} \phi(x,t) = 0, \tag{1.5}$$

with the operators M_{jk} defined as

$$M_{11} = \kappa GA\frac{\partial}{\partial x} - \rho I\frac{\partial^3}{\partial x \partial t^2} + (e_0\, a)^2 \rho I \frac{\partial^5}{\partial x^3 \partial t^2}, \tag{1.6}$$

$$M_{12} = -\kappa GA + (EI)^* \frac{\partial^2}{\partial x^2}, \tag{1.7}$$

$$M_{21} = \kappa GA\frac{\partial^2}{\partial x^2} - \rho A\frac{\partial^2}{\partial t^2} + H\frac{\partial^2}{\partial x^2} + (e_0\, a)^2 \rho A \frac{\partial^4}{\partial x^2 \partial t^2} - (e_0 a)^2 H \frac{\partial^4}{\partial x^4} \tag{1.8}$$

and

$$M_{22} = -\kappa GA\frac{\partial}{\partial x}. \tag{1.9}$$

We introduce a potential function $f(x,t)$ as follows:

$$v(x,t) = -M_{12} f(x,t) \tag{1.10}$$

and

$$\phi(x,t) = M_{11} f(x,t). \tag{1.11}$$

Substituting equations (1.10) and (1.11) into (1.4) and (1.5) makes equation (1.4) an identity. Equation (1.5) becomes

$$(M_{11}M_{22} - M_{12}M_{21}) f(x,t) = 0, \tag{1.12}$$

or

$$\begin{aligned}\Bigg[&-(\kappa GA)^2 \frac{\partial^2}{\partial x^2} + \rho I \kappa GA \frac{\partial^4}{\partial x^2 \partial t^2} - \kappa GA (e_0 a)^2 \rho I \frac{\partial^6}{\partial x^4 \partial t^2} + (\kappa GA)^2 \frac{\partial^2}{\partial x^2} - (EI)^* \kappa GA \frac{\partial^2}{\partial x^4} \\ &- \kappa GA^2 \rho \frac{\partial^2}{\partial t^2} + \rho A (EI)^* \frac{\partial^4}{\partial x^2 \partial t^2} + \kappa GAH \frac{\partial^2}{\partial x^2} - H(EI)^* \frac{\partial^4}{\partial x^4} + (e_0 a)^2 \kappa GA^2 \rho \frac{\partial^4}{\partial x^2 \partial t^2} \\ &- (e_0 a)^2 (EI)^* \rho A \frac{\partial^6}{\partial x^4 \partial t^2} - (e_0 a)^2 \kappa GAH \frac{\partial^4}{\partial x^4} + (e_0 a)^2 (EI)^* H \frac{\partial^6}{\partial x^6} \Bigg] f(x,t) = 0. \end{aligned} \tag{1.13}$$

We model the virus at the end of the beam as a concentrated mass. This mass may turn out to be either small in comparison with the mass of the beam, or large, or of the same order of magnitude as the beam's mass. In each case, different sets of boundary conditions must be adopted.

The Bresse–Timoshenko beam model for vibration analysis of carbon nanotubes was used by several authors. The interested reader may consult the studies by Wang *et al.* [14] and Elishakoff & Pentaras [15], for example. Additional references are available in the recent monograph by Elishakoff *et al.* [16].

The boundary conditions can be obtained through application of the stationarity condition of the total energy of the system. It is known that Bresse–Timoshenko theory is governed by a fourth-order differential equation for the deflection in statics or in dynamics. The non-local Bresse–Timoshenko theory leads, in fact, to a sixth-order differential equation. Two additional specific equations of the non-local terms have to be derived from variational arguments (see appendix A). For details, the interested reader must consult the monograph by Elishakoff *et al.* [10] (see also Kucuk *et al.* [16], or Adali [17], for the variational formulation of non-local Timoshenko beam problems).

The sensor is clamped at the left end, whereas at the right end, virus is attached to it. The boundary conditions read

$$\left.\begin{aligned} &v(0,t) = 0, \quad \phi(0,t) = 0, \quad v'(0,t) = 0, \quad v''(L,t) = 0, \\ &\kappa GA(v'(L,t) - \varphi(L,t)) + Hv'(L,t) - H(e_0 a)^2 v'''(L,t) + \rho A (e_0 a)^2 \ddot{v}'(L,t) \\ &\quad + M\ddot{v}(L,t) + MD\ddot{\varphi}(L,t) = 0 \\ \text{and} \quad &(EI)^* \varphi'(L,t) + (\rho I)^* (e_0 a)^2 \ddot{\varphi}'(L,t) + MD\ddot{v}(L,t) + (T + MD^2)\ddot{\varphi}(L,t) = 0, \end{aligned}\right\} \tag{1.14}$$

Table 1. Signs of coefficients in equation (1.18).

third degree	+
second degree	+ or −
first degree	+ or −
constant	+

where L is the length of the sensor, M is the mass of the virus and D is the half-length of the virus. A dot over the quantity denotes differentiation with respect to time, whereas the prime designates differentiation with respect to axial coordinate. In the case of the concentrated point mass, the size parameter D must be set to zero.

We look for the solution of equation (1.13) in the following form:

$$f(\xi, t) = F\exp(\alpha\xi)\exp(\mathrm{i}\omega t), \tag{1.15}$$

with ξ being the non-dimensional axial coordinate. The substitution of equation (1.15) into equation (1.13) results in the following polynomial equation for α:

$$\begin{aligned} &I\rho\kappa GA\alpha^2\omega^2L^4 - I\kappa GA(e_0a)^2\rho\alpha^4\omega^2L^2 + EI\kappa GA\alpha^4L^2 - \kappa GA^2\rho\omega^2L^6 + \rho AEI\alpha^2\omega^2L^4 \\ &\quad - \kappa GAH\alpha^2L^4 + HEI\alpha^4L^2 + e_0^2a^2\kappa GA^2\rho\alpha^2\omega^2L^4 - e_0^2a^2EI\rho A\alpha^4\omega^2L^2 \\ &\quad + e_0^2a^2\kappa GAH\alpha^4L^2 - e_0^2a^2EIH\alpha^6 = 0. \end{aligned} \tag{1.16}$$

We introduce the new parameter z, defined as

$$\alpha^2 = z. \tag{1.17}$$

Equation (1.16) yields

$$H(e_0a)^2(EI)^*z^3 + Cz^2 + Ez + \rho A^2\omega^2L^6\kappa G = 0, \tag{1.18}$$

with

$$\left.\begin{aligned} C &= -(EI)^*\kappa GAL^2 + \kappa GA(e_0a)^2\rho I\omega^2L^2 - H(EI)^*L^2 \\ &\quad + (e_0a)^2\rho A(EI)^*\omega^2L^2 - H(e_0a)^2\kappa GAL^2 \\ \text{and}\quad E &= -\rho I\kappa GA\omega^2L^4 + H\kappa GAL^4 - (EI)^*\rho A\omega^2L^4 - (e_0a)^2\kappa GA^2\rho\omega^2L^4. \end{aligned}\right\} \tag{1.19}$$

We would like to know the number of positive roots for this equation using Descartes' rule of signs [18]. It states that the number of positive roots equals the number of changes in sign, or that number minus an even number. The signs of the constants in each term of equation (1.18) are summarized in table 1.

Therefore, we get four combinations of the sign sequences denoted as $S1$,

$$S1 = (++++, +\,+-+, +--+, +-\,++), \tag{1.20}$$

and thus two cases: the first without change in signs, and the second with two changes in signs (last three entries in the parentheses). It means that, in the first case, equation (1.18) does not have a positive root and thus equation (1.16) does not have real roots. The second case states that there are either 2 or $2-2=0$ positive roots, i.e. Descartes' rule turns out to be inconclusive in this case.

Setting $z = -\eta$, equation (1.18) becomes

$$-H(e_0a)^2(EI)^*\eta^3 + C\eta^2 - S\eta + \rho A^2\omega^2L^6\kappa G = 0. \tag{1.21}$$

The signs of the coefficients in each term are listed in table 2.

Table 2. Signs of coefficients in equation (1.20).

third degree	−
second degree	+ or −
first degree	+ or −
constant	+

There are four possible combinations of signs $S2$,

$$S2 = (-+++, ---+, -+-+, --++). \tag{1.22}$$

Thus, using Descartes' rule of signs, we conclude that equation (1.21) has one or three positive roots, namely equation (1.21) has surely one negative root and equation (1.16) has surely two purely imaginary roots.

Moreover, we would like to analyse equation (1.16) using Cardano's analysis for cubic equations. Equation (1.18) is rewritten as

$$a_3 z^3 + a_2 z^2 + a_1 z + a_0 = 0, \tag{1.23}$$

where

$$\left.\begin{aligned} a_0 &= \rho A^2 \omega^2 L^6 \kappa G, \\ a_1 &= E = -\rho I \kappa G A \omega^2 L^4 + H \kappa G A L^4 - (EI)^* \rho A \omega^2 L^4 - (e_0 a)^2 \kappa G A^2 \rho \omega^2 L^4, \\ a_2 &= C = -(EI)^* \kappa G A L^2 + \kappa G A (e_0 a)^2 \rho I \omega^2 L^2 - H (EI)^* L^2 + (e_0 a)^2 \rho A (EI)^* \omega^2 L^2 \\ &\quad - H (e_0 a)^2 \kappa G A L^2 \\ \text{and} \quad a_3 &= H (e_0 a)^2 (EI)^*. \end{aligned}\right\} \tag{1.24}$$

We rewrite equation (1.13) as

$$y^3 + 3py + 2q = 0 \tag{1.25}$$

with substitutions

$$y = z + \frac{a_2}{3a_3}, \quad 2q = \frac{2a_2^3}{27a_3^3} - \frac{a_2 a_1}{3a_3^2} + \frac{a_0}{a_3}, \quad 3p = \frac{3a_3 a_1 - a_2^2}{3a_3^2}. \tag{1.26}$$

We define the discriminant as

$$\bar{D} = q^2 + p^3, \tag{1.27}$$

with the view to determine its sign. With the values of all the parameters, the discriminant turns out to be negative for all ω in R^+ (figure 1).

Then, equation (1.18) has surely three real roots for all ω in R^+:

$$z_k = 2\sqrt{-p}\cos\left(\frac{1}{3}\arccos\left(-q\sqrt{\frac{-1}{p^3}}\right) + \frac{2k\pi}{3}\right) - \frac{a_2}{3a_3} \quad \text{with } k \in \{1,2,3\}. \tag{1.28}$$

As verification, in figure 2, we illustrate the left-hand side of the polynomial of equation (1.25) with ω fixed at the value $\omega = 8.76 \times 10^8$ rad s^{-1}. One perfectly observes the presence of three real roots in figure 2.

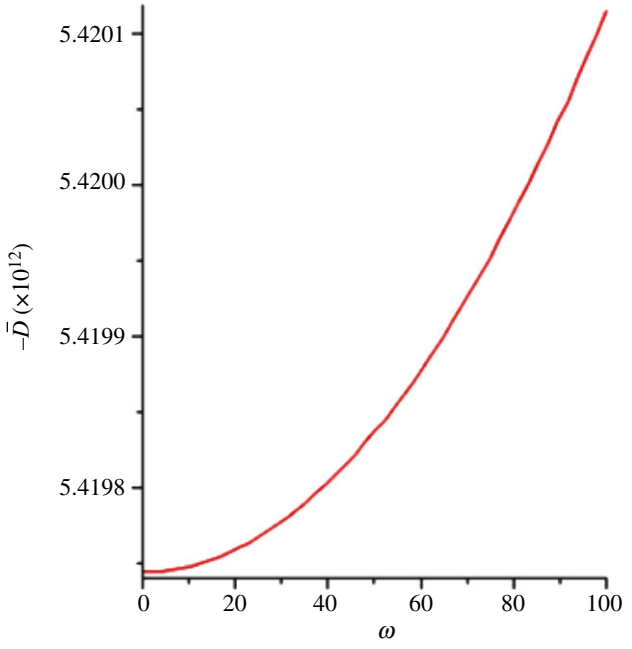

Figure 1. Variation of the discriminant $-\bar{D}$ with ω. (Online version in colour.)

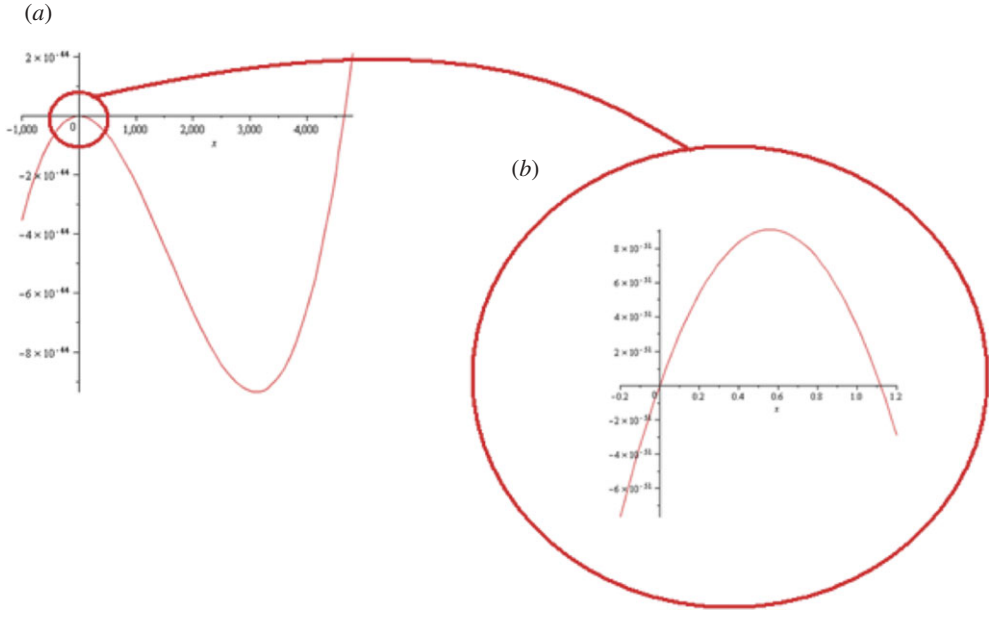

Figure 2. (*a*) Variation of the left-hand side of equation (1.25) with ω. (*b*) Zooming of the behaviour in the vicinity of $\omega = 0$. (Online version in colour.)

For the roots of this polynomial, the following results are derived:

$$\left.\begin{aligned} z_1 &= -0.000\,015\,954, \\ z_2 &= 1.118\,146\,7907 \\ \text{and} \quad z_3 &= 4652.174\,7587. \end{aligned}\right\} \tag{1.29}$$

Numerically, two roots turn out to be positive, whereas one root is negative. Let us denote them as follows:

$$z_1 = -\delta^2, \quad z_2 = \alpha^2 \quad \text{and} \quad z_3 = \beta^2, \tag{1.30}$$

where $(\alpha, \beta, \delta) \in R^3$. We arrive at the conclusion that, with equation (1.18) in mind, equation (1.13) has six solutions. Let us denote by K its set of solutions. We have

$$K = \{-\alpha, \alpha, -\beta, \beta, -\mathrm{i}\delta, \mathrm{i}\delta\}. \tag{1.31}$$

Then, using the principle of superposition, we find the solution of the problem in the following form:

$$\begin{aligned} f(\xi, t) = [&F_1 \exp(\alpha\xi) + F_2 \exp(-\alpha\xi) + F_3 \exp(\beta\xi) + F_4 \exp(-\beta\xi) \\ &+ F_5 \exp(\mathrm{i}\delta\xi) + F_6 \exp(-\mathrm{i}\delta\xi)] \exp(\mathrm{i}\omega t). \end{aligned} \tag{1.32}$$

This solution can be rewritten as

$$\begin{aligned} f(\xi, t) = [&C_1 \cosh(\alpha\xi) + C_2 \sinh(\alpha\xi) + C_3 \cosh(\beta\xi) + C_4 \sinh(\beta\xi) \\ &+ C_5 \cos(\delta\xi) + C_6 \sin(\delta\xi)] \exp(\mathrm{i}\omega t). \end{aligned} \tag{1.33}$$

Using the boundary conditions, we obtain, for each frequency ω, a homogeneous linear system of equations with respect to the constants $C_1, \ldots, C_6$. For each ω, we denote the matrix of the obtained system as $Z(\omega)$. Thus, we get the system

$$\forall \omega \in R^+, \quad [Z(\omega)]C = 0, \tag{1.34}$$

where $\forall \omega \in R^+$, $Z(\omega) \in M_6(R)$ and $C^{\mathrm{T}} = (C_1 \ C_2 \ \ldots \ C_6)$. To get non-trivial solutions, we need $\mathrm{Ker}(Z(\omega)) \neq 0$, i.e. $Z(\omega)$ has to be non-invertible, i.e. $\det(Z(\omega)) = 0$. Let us denote

$$\Omega = \{\omega \in R^+, \det[Z(\omega)] = 0\}. \tag{1.35}$$

The aim is now to find the values of ω that make the determinant of $Z(\omega)$ equal zero, i.e. the elements of Ω.

To recognize a virus, one could find a certain number of these natural frequencies and establish a spectrum of vibrations in the carbon nanotube. The expression of $Z(\omega)$ is extremely complicated, and numerically it is difficult to obtain an exact or very precise expression of the function $\omega \to \det(Z(\omega))$. So, a more affordable way to recognize a virus or bacterium is to determine the fundamental natural frequency ω_1 that makes the determinant of $Z(\omega)$ equal zero. To this end, a code has been designed to determine this first natural frequency, which is a function of both the size and the mass of the virus or bacterium. We use this code to plot $\ln(\omega_1)$ against $\ln(M)$ with D fixed, or $\ln(\omega_1)$ against $\ln(D)$ with M fixed (figures 3 and 4).

Suppose that we do not know the mass and the diameter of the virus that is attached at the tip of the cantilever sensor. Our task is to find a way to determine which virus or bacterium it is. In order to have a good approximation for the candidate virus for each measured frequency, we calculate the upper and lower bounds on the natural frequency of the system 'CNT sensor plus virus or bacterium' for each possible virus or bacterium. Note that upper and lower values are obtained rather than crisp ones, because the values of the mass and characteristic dimensions of the virus/bacterium are given in the literature as interval parameters, owing to scatter in the values of the mass density and the diameter. Hence, the calculation of the natural frequencies of the specific virus/bacterium will exhibit the associated scatter (figure 5), with natural frequencies belonging to an interval.

The lower bound of the natural frequency is determined by the maximal mass and maximal diameter, whereas the upper bound of the frequency is governed by the minimal mass and minimal diameter. The lower and upper bounds of the frequencies are listed in table 3. Note that tables S4–S8 are available in the electronic supplementary material.

Table 3. Minimum and maximum fundamental natural frequencies associated with various viruses/bacteria.

			diameter (nm)		density (kg m^{-3})		mass (kg)		frequency (rad s^{-1})	
n	virus/bacterium	shape	min	max	min	max	min	max	min	max
1	Parvoviridae	icosahedral	18	25	1390	1450	4.2445×10^{-21}	1.1863×10^{-20}	$1.2686279355 \times 10^{9}$	$2.8357694285 \times 10^{9}$
2	Tymoviridae	icosahedral	25	33	1260	1460	1.0308×10^{-20}	2.7472×10^{-20}	$6.463995065 \times 10^{8}$	$1.3609566415 \times 10^{9}$
3	Microviridae	icosahedral	25	27	1300	1400	1.0636×10^{-20}	1.4428×10^{-20}	$1.0727722835 \times 10^{9}$	$1.3398073005 \times 10^{9}$
4	Tombusviridae	icosahedral	28	35	1280	1360	1.4712×10^{-20}	3.0531×10^{-20}	$5.804988145 \times 10^{8}$	$1.0276854785 \times 10^{9}$
5	Comoviridae	icosahedral	28	30	1280	1500	1.4712×10^{20}	2.1206×10^{-20}	$8.034854275 \times 10^{8}$	$1.0276854785 \times 10^{9}$
6	Totiviridae	icosahedral	30	40	1300	1420	1.8378×10^{-20}	4.7585×10^{-20}	$4.102910365 \times 10^{8}$	$8.630942895 \times 10^{8}$
7	Nodaviridae	spherical	30	—	1300	1370	1.8378×10^{-20}	1.9368×10^{-20}	$8.407463385 \times 10^{8}$	$8.630942895 \times 10^{8}$
8	Dicistroviridae	icosahedral	30	—	1350	1370	1.9085×10^{-20}	1.9368×10^{-20}	$8.407463385 \times 10^{8}$	$8.469568575 \times 10^{8}$
9	Hepeviridae	spherical	32	34	1290	—	2.2133×10^{-20}	2.6547×10^{-20}	$6.395734455 \times 10^{8}$	$7.409921825 \times 10^{8}$
10	Picornaviridae	icosahedral	32	—	1390	—	2.3849×10^{-20}	—	$7.138363965 \times 10^{8}$	—
11	Caliciviridae	icosahedral	35	39	1330	1400	2.9858×10^{-20}	4.3483×10^{-20}	$4.395522665 \times 10^{8}$	$5.870045855 \times 10^{8}$
12	Flaviviridae	spherical	40	60	1070	1240	3.5856×10^{-20}	1.4024×10^{-19}	$1.624318715 \times 10^{8}$	$4.726570475 \times 10^{8}$
13	Hepadnaviridae	spherical	40	48	1140	1260	3.8202×10^{-20}	7.2961×10^{-20}	$2.788122575 \times 10^{8}$	$4.579140925 \times 10^{8}$
14	Tetraviridae	icosahedral	40	—	1280	1300	4.2893×10^{-20}	4.3563×10^{-20}	$4.288132275 \times 10^{8}$	$4.321493375 \times 10^{8}$
15	Papillomaviridae	icosahedral	40	55	1340	—	4.4904×10^{-20}	1.1673×10^{-19}	$1.935521795 \times 10^{8}$	$4.223617195 \times 10^{8}$
16	Polyomaviridae	icosahedral	40	55	1340	—	4.4904×10^{-20}	1.1673×10^{-19}	$1.935521795 \times 10^{8}$	$4.223617195 \times 10^{8}$
17	Reoviridae	icosahedral	60	80	1260	1440	1.4250×10^{-19}	3.8604×10^{-19}	7.41234965×10^{7}	$1.611386675 \times 10^{8}$
18	Corticoviridae	icosahedral	60	—	1290	—	1.4589×10^{-19}	—	$1.592554985 \times 10^{8}$	—
19	Tectiviridae	icosahedral	63	—	1290	—	1.6889×10^{-19}	—	$1.412219055 \times 10^{8}$	—
20	Togaviridae	spherical	70	—	1180	1200	2.1192×10^{-19}	2.1551×10^{-19}	$1.129220685 \times 10^{8}$	$1.138745215 \times 10^{8}$

(*Continued*.)

Table 3. (*Continued*.)

			diameter (nm)		density (kg m^{-3})		mass (kg)		frequency (rad s^{-1})	
n	virus/bacterium	shape	min	max	min	max	min	max	min	max
21	Birnaviridae	icosahedral	70	—	1300	1330	2.3347×10^{-19}	2.3886×10^{-19}	$1.072607485 \times 10^{8}$	$1.084918205 \times 10^{8}$
22	Orthomyxoviridae	spherical	80	120	1170	1200	3.1366×10^{-19}	1.0857×10^{-18}	2.97418545×10^{7}	8.22323075×10^{7}
23	Adenoviridae	icosahedral	80	110	1320	1350	3.5387×10^{-19}	9.4083×10^{-19}	3.47957185×10^{7}	7.74194665×10^{7}
24	Coronaviridae	spherical	120	160	1230	1240	1.1129×10^{-18}	2.6594×10^{-18}	1.43182135×10^{7}	2.93761515×10^{7}
25	Iridoviridae	polyherdal	125	300	1250	1360	1.2783×10^{-18}	1.9226×10^{-17}	2.8582535×10^{6}	2.63328805×10^{7}
26	Phycodnaviridae	icosahedral	130	200	1250	1300	1.4379×10^{-18}	5.4454×10^{-18}	8.0268545×10^{6}	2.38898055×10^{7}
27	Asfarviridae	spherical	175	215	1190	1240	3.3393×10^{-18}	6.4526×10^{-18}	6.8646005×10^{6}	1.16962195×10^{7}
28	Mimivirus	icosahedral	750	—	1360	—	3.0041×10^{-16}	—	2.904855×10^{5}	—

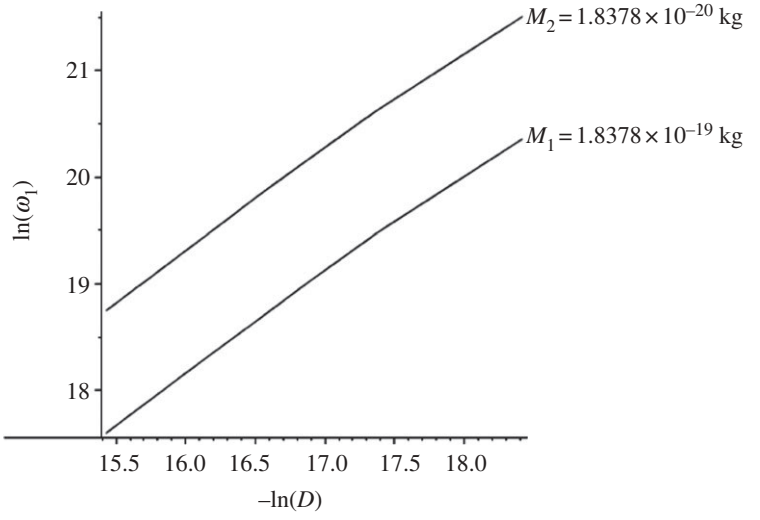

Figure 3. Variation of the natural frequency parameter ln(ω_1) with the virus/bacterium diameter parameter ln(D).

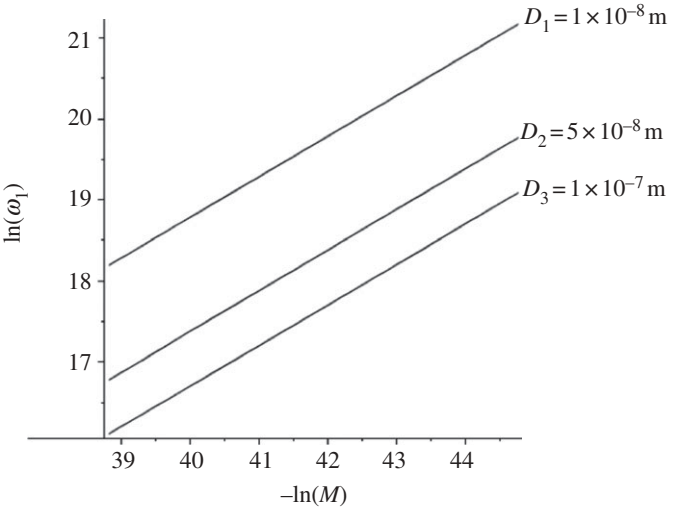

Figure 4. Variation of the natural frequency parameter ln(ω_1) with the virus/bacterium mass parameter ln(M).

Now, we have to classify the obtained natural frequencies. We choose the following steps:

1. We classify all calculated frequencies in ascending order.
2. We leave a space in table S4 between two frequency values to indicate the gap between the two frequencies obtained.
3. For each virus/bacterium, we identify the value of the minimum frequency and maximum frequency. For these two frequencies, and well as for the gap between them, we state the names of the candidate viruses/bacteria in table S4, second column.

For example, if the measured natural frequency of the system 'CNT sensor plus virus/bacterium' is $2.904\,855 \times 10^5$, then the attached virus is identified as Mimivirus. If the recorded natural frequency equals $2.858\,2535 \times 10^6$, then the attached mass is identified as Iridoviridae. In both cases, the identification process leads to a unique result. However, if the measured natural

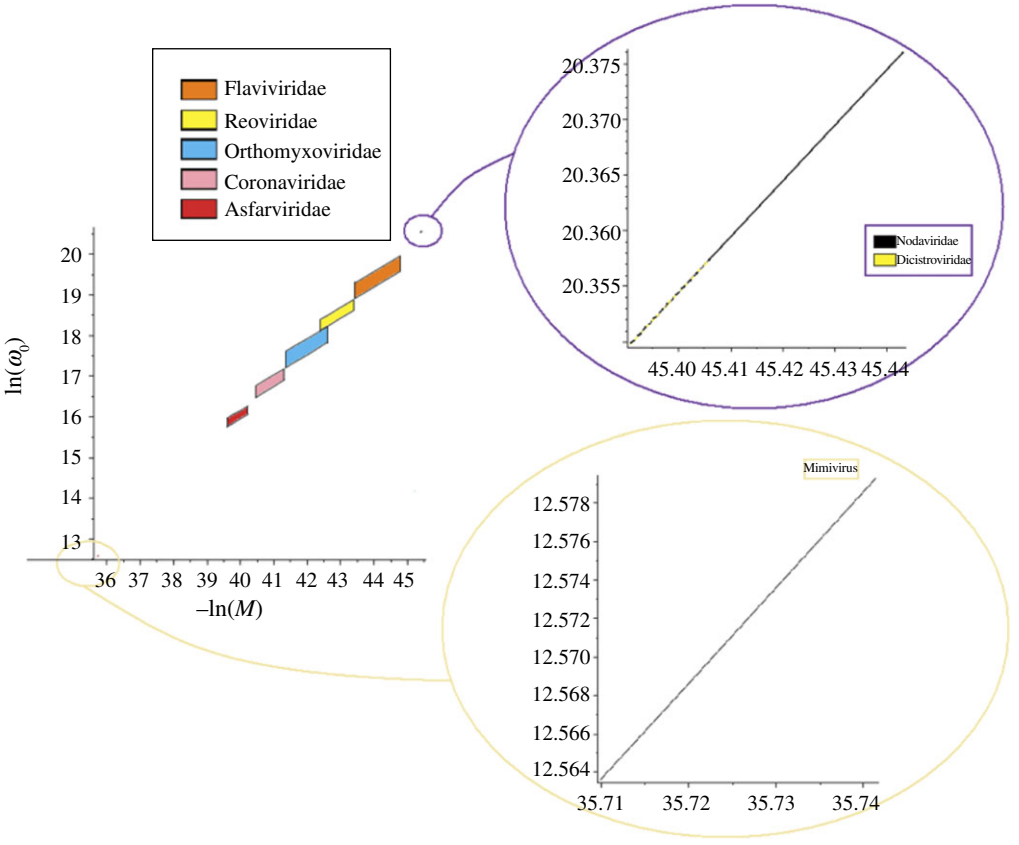

Figure 5. Variation of the natural frequency parameter with the virus/bacterium mass parameter ln(*M*) for various viruses. (Online version in colour.)

frequency equals $6.864\,6005 \times 10^6$, then there are two candidate viruses: Iridoviridae and Asfarviridae. In this case, identification does not lead to a unique result. Likewise, if the recorded natural frequency belongs to the open interval ($6.864\,6005 \times 10^6$, $8.026\,8545 \times 10^6$), the already mentioned two viruses turn out to be the candidate viruses. In the case that the measured frequency lies in the interval ($8.026\,8545 \times 10^6$, $1.169\,62195 \times 10^7$), there are three candidate viruses, namely Iridoviridae, Asfarviridae and Phycodnaviridae. In a range of considered measured frequencies, there could be at most six candidate viruses. For example, if the recorded frequency belongs to the open interval ($2.788\,122\,575 \times 10^8$, $4.102\,910\,365 \times 10^8$), there are four candidate viruses, namely Polyomaviridae, Papillomaviridae, Hepadnaviridae and Flaviviridae (see electronic supplementary material, table S5). Likewise, in the measured frequency interval ($4.288\,132\,275 \times 10^8$, $4.321\,493\,375 \times 10^8$), there are four candidate viruses, namely Tetraviridae, Hepadnaviridae, Flaviviridae and Totiviridae (see electronic supplementary material, table S6). The measured frequency interval from $5.804\,988\,145 \times 10^8$ to $8.407\,463\,385 \times 10^8$ is treated in table S7. We observe that, if the measured frequency is $8.407\,463\,385 \times 10^8$, then there are six candidate viruses, namely Dicistroviridae, Nodaviridae, Totiviridae, Comoviridae, Tymoviridae and Tombusviridae. Table S8 is associated with measured frequency interval ($8.407\,463\,385 \times 10^8$, $2.833\,769\,4285 \times 10^9$). Note that the natural frequencies are listed here with nine significant digits; such exactness naturally is unattainable in practice. In reality, the experimental set-up will determine the attainable accuracy. It is planned that the suggested methodology be implemented experimentally, starting with Mimiviruses, characterized by the journal *American Scientist* as 'giant viruses' [19,20].

2. Conclusion

In this paper, we generalized studies by Ansari & Sahmani [11], Challamel *et al.* [21], Challamel & Elishakoff [22], Liu & Rajapakse [23] and Liu *et al.* [24] to include the effects of shear deformation, rotary inertia, non-locality effect and surface effect when describing vibration of the nanosensor. It also extends the previous work performed by Elishakoff *et al.* [25], which treated the nanosensor as a Bernoulli–Euler beam, and Elishakoff *et al.* [26], which dealt with Bresse–Timoshenko nanotubes.

In this study, a theory of virus sensors based on the single-walled carbon nanotube was presented. This theory is of the Bresse–Timoshenko type, with non-local effects and surface effects included. It appears that this paper is apparently the first one for nanosensors that has incorporated the earlier-mentioned important refinements.

This work was completed when Clément Soret, Yannis Bekel and Thomas Gomez were on training programmes at the Florida Atlantic University.

Appendix A

When modelling the surface elasticity effects with a conservative load, the potential energy of the non-local Timoshenko structural system is obtained from the equivalent potential energy [10,17]:

$$U[\phi, v] = \int_0^L \left[\frac{1}{2}(EI)^*\phi'^2 + \frac{1}{2}\kappa GA(v' - \phi)^2 + \frac{1}{2}Hv'^2 + \frac{1}{2}H(e_0a)^2v''^2\right] \mathrm{d}x. \tag{A 1}$$

The kinetic energy is given by

$$\begin{aligned} T^*[\varphi, v] = &\int_0^L \left[\frac{1}{2}\rho A\dot{v}^2 + \frac{1}{2}\rho A(e_0a)^2\dot{v}'^2 + \frac{1}{2}\rho I\dot{\phi}^2\right] \mathrm{d}x \\ &+ \frac{1}{2}\rho I(e_0a)^2\dot{\phi}'^2 + \frac{1}{2}(\dot{w}(L)\dot{\varphi}(L)) \begin{pmatrix} M & MD \\ MD & T + MD^2 \end{pmatrix} \begin{pmatrix} \dot{w}(L) \\ \dot{\varphi}(L) \end{pmatrix}. \end{aligned} \tag{A 2}$$

The potential energy has been enriched, thanks to the non-local term, whereas the gradient of the kinematic variables is involved in the modified kinetic energy. With this formulation, the non-local model is presented as a generalized gradient model, with generalized inertia terms. This equivalence was already discussed by Challamel *et al.* [21].

By application of Hamilton's principle to the modified Hamiltonian $\int_{t_1}^{t_2}(\delta U^* - \delta T^*)\,\mathrm{d}t = 0$, the following partial differential equations are obtained (see also Lee & Chang [8]):

$$\left.\begin{aligned} &(EI)^*\frac{\partial^2\phi}{\partial x^2} + \kappa GA\left(\frac{\partial v}{\partial x} - \phi\right) - \left[1 - (e_0a)^2\frac{\partial^2}{\partial x^2}\right](\rho I)^*\frac{\partial^2\phi}{\partial t^2} = 0 \\ \text{and}\quad &\kappa GA\left(\frac{\partial^2 v}{\partial x^2} - \frac{\partial\phi}{\partial x}\right) - \left[1 - (e_0a)^2\frac{\partial^2}{\partial x^2}\right]\left[(\rho A)^*\frac{\partial^2 v}{\partial t^2} - H\frac{\partial^2 v}{\partial x^2}\right] = -\left[p - (e_0a)^2\frac{\partial^2 p}{\partial x^2}\right], \end{aligned}\right\} \tag{A 3}$$

where $p = 0$ in the present study.

The natural and essential boundary conditions of the problem are detailed below:

$$\left.\begin{aligned} &[\{(EI)^*\phi' + (\rho I)^*(e_0a)^2\ddot{\phi}'\}\delta\phi]_0^L + [MD\ddot{v}(L) + (T + MD^2)\ddot{\phi}(L)]\delta\phi(L) = 0, \\ &[\{\kappa GA(v' - \phi) + Hv' - H(e_0a)^2v''' + \rho A(e_0a)^2\ddot{v}'\}\delta v]_0^L + [M\ddot{v}(L) + MD\ddot{\phi}(L)]\delta v(L) = 0 \\ \text{and}\quad &[H(e_0a)^2v''\delta v']_0^L = 0. \end{aligned}\right\} \tag{A 4}$$

For a clamped–free nanobeam, the boundary conditions of the non-local Timoshenko beam in the presence of conservative surface elasticity load are

$$\left.\begin{aligned}
&\phi(0) = 0,\\
&(EI)^*\phi'(L) + (\rho I)^*(e_0a)^2\ddot{\phi}'(L) + MD\ddot{v}(L) + (T + MD^2)\ddot{\phi}(L) = 0,\\
&v(0) = 0,\\
&\kappa GA(v'(L) - \phi(L)) + Hv'(L) - H(e_0a)^2v'''(L) + \rho A(e_0a)^2\ddot{v}'(L) + M\ddot{v}(L) + MD\ddot{\phi}(L) = 0,\\
&v'(0) = 0\\
\text{and}\quad &H(e_0a)^2v''(L) = 0.
\end{aligned}\right\} \tag{A 5}$$

These boundary conditions are the ones used in this paper.

For a clamped–free nanobeam with surface elasticity effects modelled as a non-conservative loading (see Challamel & Elishakoff [12]), the boundary conditions of the non-local Timoshenko beam in the presence of non-conservative surface elasticity load are

$$\left.\begin{aligned}
&\phi(0) = 0,\\
&(EI)^*\phi'(L) + (\rho I)^*(e_0a)^2\ddot{\phi}'(L) + MD\ddot{v}(L) + (T + MD^2)\ddot{\phi}(L) = 0,\\
&v(0) = 0,\\
&\kappa GA(v'(L) - \phi(L)) - H(e_0a)^2v'''(L) + \rho A(e_0a)^2\ddot{v}'(L) + M\ddot{v}(L) + MD\ddot{\phi}(L) = 0,\\
&v'(0) = 0\\
\text{and}\quad &H(e_0a)^2v''(L) = 0.
\end{aligned}\right\} \tag{A 6}$$

References

1. Tibbals HF. 2010 *Medical nanotechnology and nanomedicine*. Boca Raton, FL: CRC Press.
2. Koprowski G. 2011 *Nanotechnology in medicine: emerging applications*. New York, NY: McGraw-Hill.
3. Jha AR. 2008 *MEMS and nanotechnology-based sensors and devices for communications, medical, and aerospace applications*. Boca Raton, FL: CRC Press.
4. Khanna VK. 2011 *Nanosensors: physical, chemical, and biological*. Boca Raton, FL: CRC Press.
5. Lim T-C. 2010 *Nanosensors: theory and applications in industry, healthcare and defence*. Boca Raton, FL: CRC Press.
6. Lu P, Lee HP, Lu C, Zhang PQ. 2006 Dynamic properties of flexural beams using a nonlocal elasticity model. *J. Appl. Phys.* **99**, 073510. (doi:10.1063/1.2189213)
7. Lu P, Lee HP, Lu C, Zhang PQ. 2007 Application of nonlocal beam models for carbon nanotubes. *Int. J. Solids Struct.* **44**, 5289–5300. (doi:10.1016/j.ijsolstr.2006.12.034)
8. Lee HL, Chang WJ. 2010 Surface effects on the frequency analysis of nanotubes using nonlocal Timoshenko beam theory. *J. Appl. Phys.* **108**, 093503. (doi:10.1063/1.3503853)
9. Lei XW, Natsuki T, Shi J, Ni QQ. 2012 Surface effects on the vibrational frequency of double-walled carbon nanotubes using the nonlocal Timoshenko beam model. *Composites B: Eng.* **43**, 64–69. (doi:10.1016/j.compositesb.2011.04.032)
10. Elishakoff I *et al.* 2012 *Carbon nanotubes and nanosensors: vibrations, buckling and ballistic impact*. London, UK: ISTE; and Hoboken, NJ: Wiley.
11. Ansari R, Sahmani S. 2011 Bending behaviour and buckling of nanobeams including surface stress effects corresponding to different beam theories. *Int. J. Eng. Sci.* **49**, 1244–1255. (doi:10.1016/j.ijengsci.2011.01.007)
12. Challamel N, Elishakoff I. 2011 Surface elasticity effects can apparently be explained via their non-conservativeness. *ASME J. Nanotechnol. Eng. Med.* **2**, 031008. (doi:10.1115/1.4005486)
13. Elishakoff I. 2010 An equation both more consistent and simpler than the Bresse–Timoshenko equation. In *Advances in mathematical modeling and experimental methods for materials and structures* (eds R Gilat, L Banks-Sills), pp. 249–254. Berlin, Germany: Springer.
14. Wang CM, Tan VBC, Zhang YY. 2006 Timoshenko beam model for vibration analysis of multi-walled carbon nanotubes. *J. Sound Vib.* **294**, 1060–1072. (doi:10.1016/j.jsv.2006.01.005)

15. Elishakoff I, Pentaras D. 2009 Natural frequencies of carbon nanotubes based on simplified Bresse–Timoshenko theory. *J. Comput. Theor. Nanosci.* **6**, 1527–1531. (doi:10.1166/jctn.2009.1206)
16. Kucuk I, Sadek IS, Adali S. 2010 Variational principles for multiwalled carbon nanotubes undergoing vibrations based on nonlocal Timoshenko beam theory. *J. Nanomater.* **2010**, 461252. (doi:10.1155/2010/461252)
17. Adali S. 2012 Variational formulation for buckling of multi-walled carbon nanotubes modelled as nonlocal Timoshenko beams. *J. Theor. Appl. Mech.* **50**, 321–333.
18. Korn GA, Korn TM. 1961 *Mathematical handbook for scientists and engineers*. New York, NY: McGraw-Hill.
19. Claverie JM, Abergel C. 2009 Mimivirus and its virophage. *Annu. Rev. Genet.* **43**, 8–13. (doi:10.1146/annurev-genet-102108-134255)
20. Van Etten JL. 2011 Giant viruses. *Am. Sci.* **99**, 304–311. (doi:10.1511/2011.91.304)
21. Challamel N, Rakotomanana L, Le Marrec L. 2009 A dispersive wave equation using non-local elasticity. *C. R. Mécanique* **337**, 591–595. (doi:10.1016/j.crme.2009.06.028)
22. Challamel N, Elishakoff I. 2012 Surface stress effects may induce softening: Euler–Bernoulli and Timoshenko buckling solutions. *Physica E* **44**, 1862–1867. (doi:10.1016/j.physe.2012.05.019)
23. Liu C, Rajapakse RKND. 2010 Continuum models incorporating surface energy for static and dynamic response of nanoscale beams. *IEEE Trans. Nanotechnol.* **9**, 422–431. (doi:10.1109/tnano.2009.2034142)
24. Liu C, Rajapakse RKND, Phani AS. 2011 Finite element modelling of beams with surface energy effects. *J. Appl. Mech.* **78**, 031014. (doi:10.1115/1.4003363)
25. Elishakoff I, Versaci C, Muscolino G. 2011 Clamped–free double walled carbon nanotube-based mass sensor. *Acta Mech.* **219**, 29–43. (doi:10.1007/s00707-010-0435-1)
26. Elishakoff I, Ghyselinck G, Bucas S. 2012 Virus sensor based on a single-walled carbon nanotube treated as Bresse–Timoshenko beam. *J. Appl. Mech.* **79**, 064502. (doi:10.1115/1.4006492)